Catalysis Today 144 (2009) 306–311

Contents lists available at ScienceDirect

Catalysis Today

journal homepage: www.elsevier.com/locate/cattod

Bimetallic catalysts for the catalytic combustion of methane using microreactor technology

M. O'Connell [a,*], G. Kolb [a], R. Zapf [a], Y. Men [a], V. Hessel [a,b]

[a] Institut für Mikrotechnik Mainz GmbH, Carl-Zeiss-Straße 18-20, 55129 Mainz, Germany
[b] Department of Chemical Engineering and Chemistry, Eindhoven University of Technology (TU/e), Den Dolech 2, Postbus 513, 5600 MB, Eindhoven, The Netherlands

ARTICLE INFO

Article history:
Available online 25 December 2008

Keywords:
Microchannels
Combustion
Methane
Platinum
Alumina
Molybdenum
Tungsten

ABSTRACT

Pt–W and Pt–Mo based catalysts were evaluated for methane combustion using a sandwich-type microreactor. Alumina washcoated microchannels were impregnated with platinum in combination with and promoted with tungsten and molybdenum and compared with commercially available Pt/Al_2O_3 catalysts. Catalysts were tested in the range of 300–700 °C with flow rates adjusted to GHSV of 74,000 h^{-1} and WHSV of 316 L h^{-1} g^{-1}. Catalysts containing tungsten were found to be the most active and the most stable possibly due to a metal interaction effect. A Pt–W/γ-Al_2O_3 containing 4.6 wt% Pt and 9 wt% W displayed the highest activity with full conversion at 600 °C and a selectivity to CO_2 of 99%.

1. Introduction

For more than 30 years, many investigations have been conducted into elucidating the intrinsic details of the catalytic combustion of methane [1–6]. The reasons for this are two-fold, namely for pollution abatement and for power generation. Methane is a by-product in many industrial processes and is also a pollutant from automobiles and gas power plants. Automotive applications require fuel cells with high power and efficiency, low operational costs, long durability of components, and compact dimensions. Proton exchange membrane (PEM) fuel cells are usually applied in cars because they are small and light, they operate at a relatively low temperature and they are operationally flexible. A fuel cell, which uses pure hydrogen as fuel, produces only steam with zero polluting emissions; however, for mobile applications, apart from the high cost of the on-board tanking, a major drawback which is hindering the application of the technology is the lack of infrastructure for pure hydrogen refueling. It is generally agreed that the only viable way to produce hydrogen, in large enough quantities to satisfy demand now and in the future, is via hydrocarbon conversion processes (usually petrol and diesel oils). Normally, this is achieved by autothermal reforming (ATR) and steam reforming (SR), resulting in hydrogen-rich gases.

Multifunctional reactors hosting catalytic combustion and steam reforming of fuel at the opposite sides of a heat-exchanger appear to be very promising for achieving maximum compactness, a very desirable property for an auxiliary power unit placed on-board road vehicles, yachts, and aircrafts. Microchannel reactors can satisfy this requirement because of their enhanced heat and mass transfer characteristics, the flow uniformity, the high surface area to volume ratio, safe control in explosive regimes and easier scale-up possibilities [7]. Microchannel fuel processors containing catalytic combustors have been recently developed [8–10]. Methane and diesel were used for combustion for preheating the future systems. The anode-off gases containing hydrogen and methane can be introduced into the combustor as a fuel during normal operation.

Many studies have been done into addressing both the design and manufacture of suitable catalysts for the combustion process and the fabrication of unique but efficient reactors so as to maximize the effectiveness of these active catalysts. Invariably, the majority of the most active combustion catalysts consist of an active constituent and a support. Perovskites [11] doped metal oxides [12] and hexaluminates [13] have all been utilized for catalytic combustion, but the majority of the studies have involved noble metal based catalysts [[14] and references therein]. Relative to oxide catalysts, precious metal catalysts possess a greater resilience against sintering and a higher resistance to sulfur poisoning, but more importantly a higher specific catalytic activity that renders them attractive as potential catalysts for catalytic combustion. They can be manufactured in a highly dispersed state

* Corresponding author.
E-mail address: oconnell@imm-mainz.de (M. O'Connell).

0920-5861/$ – see front matter © 2008 Elsevier B.V. All rights reserved.
doi:10.1016/j.cattod.2008.10.053

on standard supports like silica and alumina, thus leading to improved activity.

With respect to Pt catalysts promoted with Mo and W, Yazawa et al. [15] showed that the activity of such catalysts for propane combustion was much enhanced, which was ascribed to the electronic properties of molybdenum and tungsten. The activity of Pt is mainly influenced by its oxidation state, with higher activities seen when Pt is less oxidized. Effectively, the electron deficiency of platinum varies with the electronegativity of additives, and the higher electronegativity enhances the electron deficiency of platinum, but depresses the oxidation of Pt. da Silva and Schmal [16] suggested that a synergy exists between Mo and Pt/Al_2O_3, which were studied for NO reduction by CO. Molybdenum helps to stabilize both the Pt and Al_2O_3 by enhancing the oxygen storage capacity and spillover effect, while on the other hand platinum maintains the surrounding molybdenum particles in its more active form. It has also been suggested [17] from density functional theory studies that MoO_3^- supported Pt catalysts can facilitate single C–H bond activation in methane.

Yatsimirskii et al. investigated the oxidation of H_2 [18] and of CO [19] for 0.5 wt% Pt/WO_3 catalysts and found that the enhancement in activity could be attributed to the formation of oxide bronzes, the subsequent interaction between these bronzes and the metallic Pt, and the appearance of oxygen vacancies.

Hua and Sommer [20] studied *n*-heptane isomerization over Al_2O_3-doped $Pt/WO_x/ZrO_2$ and found that the catalytic activity depends strongly on surface WO_x loading and were attributed to an increase in the number of Brønsted acid sites. The maximum activity was observed at a WO_x concentration of 10 wt% W, which was slightly higher than the theoretical monolayer capacity.

In this work, $Pt/\gamma\text{-}Al_2O_3$ catalysts promoted by W and Mo were prepared and assessed for their effectiveness for the catalytic combustion of methane. It is clear that the catalytic behavior of these systems is controlled by complex mechanisms, therefore characterization studies were also performed so as to develop a better perspective on the solid state behavior of these catalysts and concurrently to relate this to the catalytic activity.

2. Experimental

2.1. Preparation and characterization of catalysts

The home-made catalyst coatings were based upon pure alumina carriers. The catalysts were prepared by washcoating alumina into the microchannels. This was achieved by manually filling the microchannels with alumina suspension. This was then followed by drying at room temperature and a calcination step at 600 °C. Incipient wetness impregnation was then performed in the following manner. The support was doubly impregnated, firstly with a certain amount of Pt (as tetramine platinum (II) nitrate) which was calcined at 450 °C and similarly then with W or Mo (as aqueous metal salt solutions, namely ammonium tungstate and ammonium molybdate, respectively). This was then followed by a drying and a final calcination step at 400 °C.

The commercial catalysts were based upon commercial Pt/Al_2O_3 catalysts supplied from Degussa (F214 SP/D 5%). These were similarly introduced into the microchannels by a sequential washcoating, drying and calcination (at 450 °C) procedure. W or Mo was then impregnated followed by drying and calcining at 400 °C. A more detailed description of the washcoating procedure can be obtained from the previous studies [21].

The specific surface area was determined by nitrogen sorption using a Sorptomatic 1990 (Carlo Erba Instruments) automatic apparatus and calculated by the BET method. XRD measurements were performed on samples placed in glass capillaries using a Siemens D5000 diffractometer with Cu Kα radiation (λ = 1.54 Å) in Debye–Scherrer geometry (capillary technique) and a position sensitive detector. Samples were scanned from 5° to 105° with a step size of 0.079° and a step time of 10 s. IR measurements were performed using a Bruker FT-IR spectrometer IF66SV in a measurement ranging from 400 to 4000 cm^{-1}. The resolution of the measurement was 1.928 cm^{-1}. Each sample was scanned 200 times and the signal averaged.

2.2. Catalyst testing

Experiments were performed in sandwich-type reactors composed of two laser-welded microstructured platelets, each having 14 channels with 500 μm width and 250 μm depth, which were described in more detail in previous studies [22]. The microchannels were etched by means of wet-chemical etching using aqueous iron chloride solutions. Inlet and outlet capillaries were attached to the reactors by laser welding. A depiction of the reactor can be seen in Fig. 1, before and after laser welding. The dimensions of the microreactor were measured to be 51 cm long and 14 cm wide, with the catalyst coating being of 40 μm depth. The microreactors were placed into a metal block powered by a heating cartridge regulated by a PID temperature controller with a K-type thermocouple inserted next to the bed of the catalyst. Temperature differences between the gas outlet temperature and the reactor temperature were less than 2 °C. As the heating block was also insulated, isothermal behavior of the reactor was assumed. The temperature range for testing was 300–700 °C.

For the gas supply, mass flow controllers for methane and synthetic air (BRONCKHORST HI-TEC) were used. After two samples were taken for analysis, the temperature was increased by 50 °C until a final temperature of 700 °C was reached. Subsequently, the mid-term stability of the catalyst (100 h) was measured. Experiments were carried out at a λ number of 1.1, i.e. the O/C ratio was 2.2. Flow rates were typically adjusted to a total flow rate of 107 mL min^{-1} with respect to the reactants, resulting in a GHSV of 74,000 h^{-1} (here defined as the ratio of the volumetric

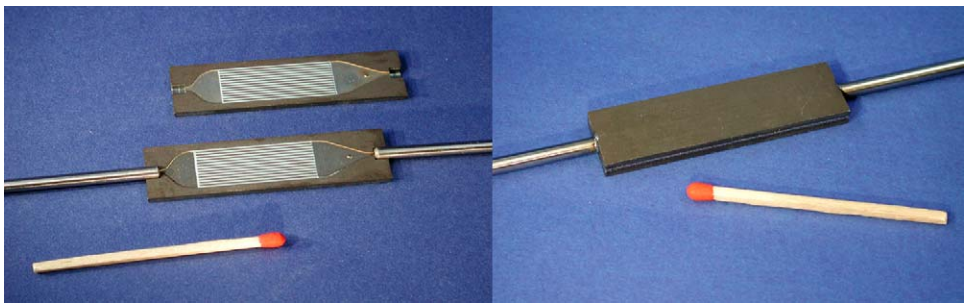

Fig. 1. Depiction of the microchannel reactor platelets used for the methane combustion reaction.

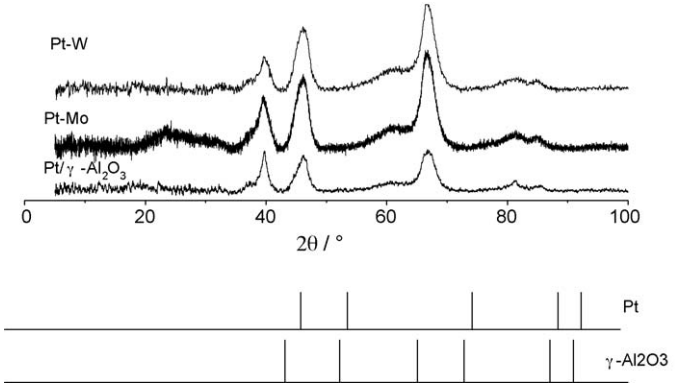

Fig. 2. PXRD's for catalysts prepared via the commercial process, W_{comm} and Mo_{comm}. Due to the overlapping nature of the Pt and Al_2O_3 peaks, also shown are tick marks representing: (a) Pt peak positions, taken from JCPDS 4-802 and (b) γ-Al_2O_3 peak positions, taken from JCPDS 74-2206.

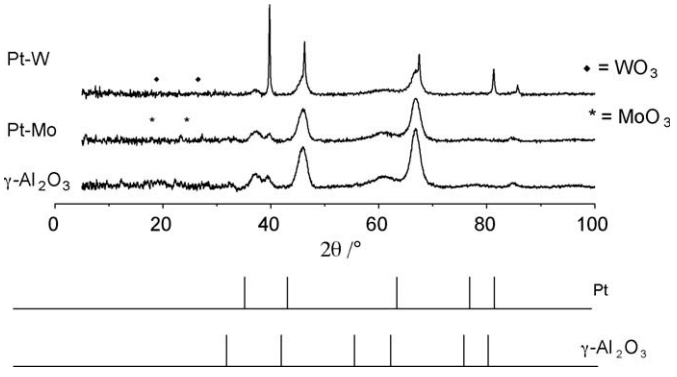

Fig. 3. PXRD's for catalysts prepared via the home-made process, W_{home} and Mo_{home}. Due to the overlapping nature of the Pt and Al_2O_3 peaks, also shown are tick marks representing: (a) Pt peak positions, taken from JCPDS 4-802 and (b) γ-Al_2O_3 peak positions, taken from JCPDS 74-2206.

flow rate of the feed stream at STP to the volume of the coated channels) and a WHSV of 316 L h^{-1} g^{-1}. The CH_4 flow rate was 9.74 mL min^{-1}, so the CH_4 concentration in air was 9.1 vol%.

Product gases were analyzed by an on-line automated gas chromatograph (Trace GC, Thermo-Finnigan). The two-channel GC was equipped with a pre-column Porapak N, a Haysep Q column, a molecular sieve 5A column, and a combined Haysep and molsieve column. On both channels the concentrations were determined by thermal conductivity detectors.

3. Results and discussion

3.1. Textural properties of catalysts

Textural properties and catalyst compositions are illustrated in Table 1. When commercial versus home-made catalysts are compared, the commercial based catalysts always have an enhanced surface area relative to the home based. When W versus Mo promoted catalysts are compared, it can be seen that Mo always has a larger surface area relative to W. Machida and co-workers [23] concluded from studies on Pt–M, co-exchanged hydrotalcite systems, M = W or Mo, that lower surface areas are a consequence of pore blockage caused by the deposition of Mo or W oxides.

3.2. Catalyst characterization

Figs. 2 and 3 depict XRD spectra for the commercial and home-made samples, respectively. For all samples, there were no major peaks attributable to both Mo and W, irrespective of the preparation method. Another notable feature is that catalysts prepared from the commercial base catalyst were even less crystalline relative to their home-made equivalents. There is evidence for Pt presence with major $\theta/2\theta$ peaks at 39.5°, 46°, 67.5° and 81°, but this is difficult to quantify exactly given the proximity of these peaks to those of alumina. At higher age temperatures it is possible that this becomes easier to establish and distinguish. There are no significant peaks which are characteristic of a reduced or oxidized Pt phase, indicating a high dispersion of Pt.

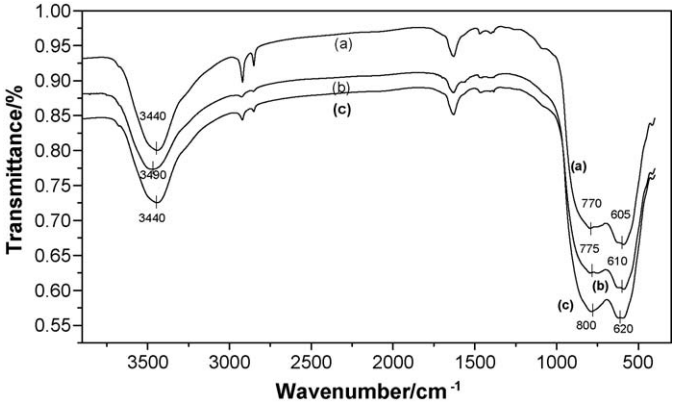

Fig. 4. IR spectra for (a) Mo_{comm}, (b) Pt/Al_2O_3 and (c) W_{comm}.

Since the XRD data provided little information about the nature of the active metal content in the catalysts, FT-IR measurements were performed. Figs. 4 and 5 present IR spectra for both the commercial and home-made catalysts, respectively, together with Pt/Al_2O_3 and Al_2O_3 spectra as references. Two significant features are noteworthy here. Firstly, both the home and commercial based catalysts exhibit a shift of up to 50 cm^{-1} in the hydroxyl peak of 3500 cm^{-1} relative to the Pt/Al_2O_3 standard. This is consistent with the presence of weak Pt–W (or Mo) interactions, which is likely to involve only a small amount of Pt atoms and W or Mo cations. Secondly, further evidence for the existence of these weak interactions can be seen on close inspection of the region below 1000 cm^{-1}, the fingerprint region for both Al–OH translation modes and M–O skeletal vibrations [24]. For example, in the Mo spectra, the band at 620 cm^{-1} can be ascribed to characteristic Mo–O–Mo bridging bonds [25]. Octahedral MoO_3 is IR active in both the 800–990 cm^{-1} region and at 570 cm^{-1}. For WO_3, these vibrations can lie between 720 and 920 cm^{-1} [26].

While the shifts in wave number are small in comparison to above and within the experimental uncertainty (of the order of

Table 1
Textural properties and catalyst compositions for all catalysts studied.

Sample	Code in text	% Pt (wt%)	% W (wt%)	% Mo (wt%)	Surface area (m^2 g^{-1})	Pore volume (cm^3 g^{-1})
Pt–W/γ-Al_2O_3 commercial	W_{comm}	4.6	9	0	214	0.754
Pt–W/γ-Al_2O_3 home	W_{home}	4.6	9	0	123	0.385
Pt–Mo/γ-Al_2O_3 commercial	Mo_{comm}	4.6	0	9	242	0.854
Pt–Mo/γ-Al_2O_3 home	Mo_{comm}	4.6	0	9	150	0.372

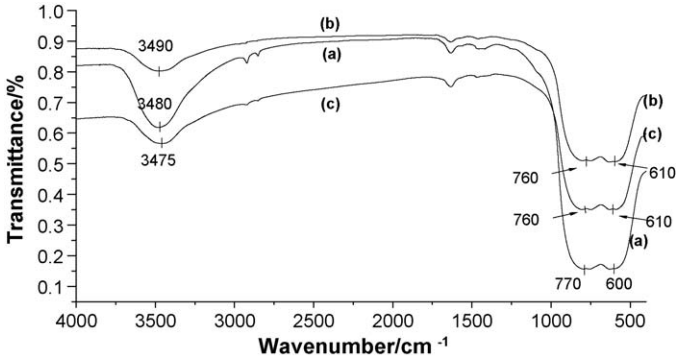

Fig. 5. IR spectra for (a) Al_2O_3, (b) Mo_{home} and (c)W_{home}.

10 cm^{-1}), the original double peak seen below 1000 cm^{-1} for both Pt/Al_2O_3 and Al_2O_3 is further split into two more doublets, which must be as a consequence of the W and Mo introduction. Other minor peaks are present at 1630 cm^{-1}, possibly a hydroxyl bending mode and at 1450 cm^{-1}, which is typical of adsorbed carbonates on the surface of mixed oxides formed during calcination [27].

3.3. Primary catalyst screening

Conversion curves for all four catalysts tested are illustrated in Fig. 6, while the temperatures required to achieve different degrees of conversion and selectivities are summarized in Table 2. The absence of heat and mass transfer limitations in microreactor technology allows for its utilization in highly exothermic reactions due to the suppression of hot spot formation. As can be seen, catalysts containing W have higher activities than Mo with T_{50} values (i.e. the temperature at which 50% conversion is achieved), showing an enhanced activity of 25 °C. It must be noted here that under the reaction conditions studied, i.e. in a slight oxygen excess, full selectivity towards CO_2 was never seen. W_{comm} showed the best activity for methane combustion with a lowest T_{50} of 493 °C. It is possible that this improvement in the activity is due to metal interaction effects. This was seen in IR measurements (as discussed previously) and in XRD measurements. Taking for example the $\theta/2\theta$ peak centered on 46°, the particle size is larger, possibly due to the presence of weaker Pt–support interactions and a corresponding increase in Pt–W interaction. M'Boungou et al. [28] have measured the improved activity for the reforming of 3-methylhexane at similar concentrations of W, which they believe is accounted for by

Table 2
Temperature required to achieve 10, 50 and 100% conversion respectively together with selectivity values (at the temperature for 100% conversion) for all catalysts studied. λ = 1.1, Q_{tot} = 107 mL min^{-1}, GHSV of 74,000 h^{-1} and WHSV of 316 L h^{-1} g^{-1}.

Sample	T_{10} (°C)	T_{50} (°C)	T_{100} (°C)	Selectivity CO_2 (%)
Pt–W/γ-Al_2O_3 commercial	399	493	600	99
Pt–W/γ-Al_2O_3 home	430	528	625	99
Pt–Mo/γ-Al_2O_3 commercial	443	526	625	99
Pt–Mo/γ-Al_2O_3 home	470	554	650	99

a synergistic effect. This is due to the interactions between Pt° and W rather than the classical Pt°–Al_2O_3 interaction. However, it should be noted that there the support was first impregnated with W and then Pt, whereas here it is in the reverse order. Alexeev et al. [29] showed that for the hydrogenation of crotonaldehyde to crotyl alcohol Pt–W catalysts were more active than Pt/γ-Al_2O_3 because it appeared that tungsten formed microscopic islands on γ-Al_2O_3 influencing the adsorption and catalysis by platinum. Here, as both active species are well dispersed on the surface of the catalyst, synergetic effects can explain its behavior. For propane combustion, Yoshida et al. [30] demonstrated that the total electrophilicity of the support and additives can improve the oxidation resistance of Pt, leading to higher activities. W and Mo, having electronegativities of 2.92 and 2.96, respectively, displayed the highest activity for propane combustion, over an alumina support, with tungsten displaying the highest propane conversion.

Of course, particle size effects should not be ruled out. It has been shown that there are different reactivities of adsorbed oxygen on the platinum surface [14]. Two types of platinum particles can exist on the surface of the support, namely, completely dispersed platinum where platinum can be oxidized to PtO_2, and platinum crystallites where oxygen is adsorbed on the crystallites to generate highly reactive adsorbed oxygen. On comparing the peak widths from the XRD spectra in Figs. 2 and 3, it can be seen that the W_{home} catalyst has a larger particle size compared with its Mo equivalent. Hicks [31] also noted that the rate of catalytic combustion can increase with increasing Pt particle size, at least up to a certain limit. However, it should be noted that the catalysts here were prepared from non-Cl precursors, which was not the case for the studies referred to above.

When the Mo catalysts are compared with their W equivalents, it was observed that Pt–Mo based catalysts are less active for methane combustion. Even though for Pt–Mo the surface areas are high, there is a strong and direct correlation between Pt dispersion

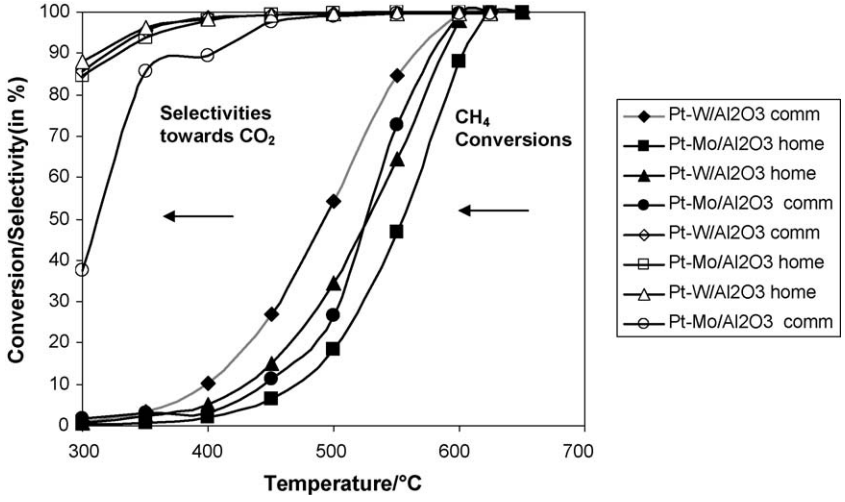

Fig. 6. Methane conversion and selectivities for all four catalysts tested. λ = 1.1, Q_{tot} = 107 mL min^{-1}, GHSV of 74,000 h^{-1} and WHSV of 316 L h^{-1} g^{-1}.

and catalytic performance for these kinds of catalysts. There is also slight evidence from XRD data that a very small amount of Mo has segregated out as orthorhombic MoO_3 for the Mo_{home} catalyst, which is the worst performing catalyst, indicating that the level of dispersion of Mo is lower relative to the other catalysts and that relatively large crystallites of Mo exist on the alumina support material. However, given the large signal to noise ratio seen in the diffraction studies, further characterization studies need to be performed to confirm this. The larger the degree of dispersion of the Mo particles, the better the catalytic activity, as the higher active surface provides more effective contact with the reactants.

It has been shown for the Pt–W equivalent [28] that when there is a large degree of segregation, the extent of intermetallic interaction is minimal. Pinzon et al. [32] have shown that platinum dispersion for these catalysts is enhanced at a low and specific metal composition, i.e. Pt/(Pt + Mo) = 0.14 (compared to 0.34 in this study), promoting a synergy effect between Pt and Mo. Leclercq et al. [33] believe that the nature of the active site in Pt–Mo based catalysts is not stable and changes with the nature of the reacting mixture in contact with it and adapts itself to the reaction. They found that, after a pre-reduction treatment which can induce a molybdenum surface enrichment effect, only a constant fraction of Pt is accessible at the surface. This is especially true in the presence of oxygen at high temperature (as is present here). When the same promoters are compared, commercial based catalysts outperform home based catalysts both times, which can be attributed to an increase in the surface area.

3.4. Subsequent catalyst screening

The most active catalyst for the primary screening, W_{comm}, was then tested for a second run under similar conditions to the initial tests. Results for this can be seen in Fig. 7. On comparison to the T_{50} values, it was observed that the catalyst had already deactivated by 40 °C. Similar results have previously been seen for Pt/Al_2O_3 catalysts [34]. Burch and Loader [35] have shown that the extent of oxidation of the platinum surface is a key factor on the catalytic behavior, a more oxidized platinum surface being less active relative to a less oxidized surface. Operating then under oxygen rich conditions, as was performed here, should then raise the oxidation extent of the Pt surface.

Although many hundreds of studies are available on methane combustion, not many of these deal with longer term testing. W_{comm} catalyst was then tested for a mid-term test lasting 100 h. When the fresh catalyst was tested, full conversion was observed

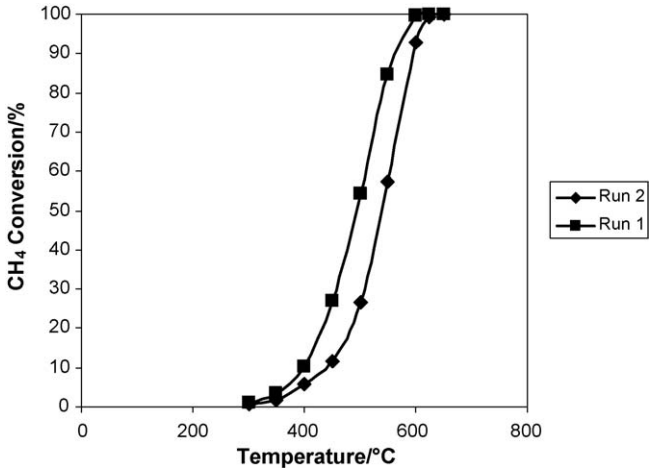

Fig. 7. Methane conversion for W_{comm}, after two complete cycles. λ = 1.1, Q_{tot} = 107 mL min^{-1}, GHSV of 74,000 h^{-1} and WHSV of 316 L h^{-1} g^{-1}.

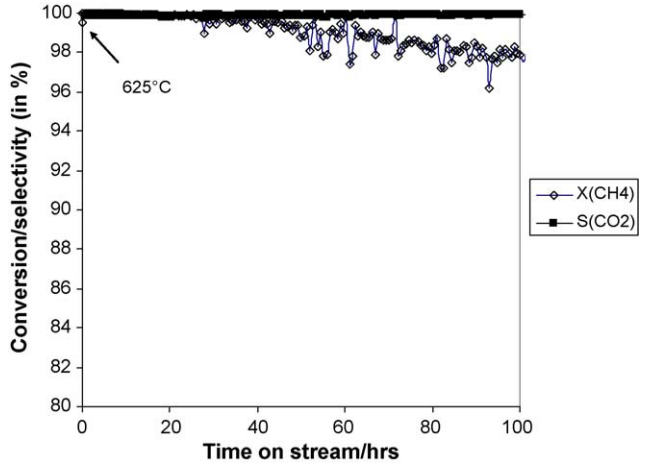

Fig. 8. 100 h test at 635 °C for W_{comm}. λ = 1.1, Q_{tot} = 107 mL min^{-1}, GHSV of 74,000 h^{-1} and WHSV of 316 L h^{-1} g^{-1}.

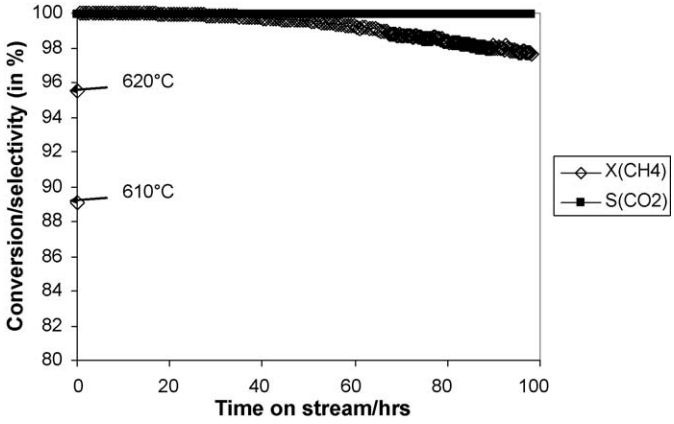

Fig. 9. 100 h test at 660 °C for Mo_{comm}. λ = 1.1, Q_{tot} = 107 mL min^{-1}, GHSV of 74,000 h^{-1} and WHSV of 316 L h^{-1} g^{-1}.

at 600 °C, but after exposure to 2 reaction cycles it was found that full conversion was not achieved until 635 °C. At 625 °C, 99.53% conversion was observed. Results for this run are seen in Fig. 8. 100% conversion was achieved for the first 60 h of operation after which the catalyst began to slowly deactivate, culminating in a conversion of 98% after 100 h. This compares favorably with other studies, e.g. Barbosa et al. [36] achieved 80% conversion for methane combustion after 100 h over unsupported iron oxide catalysts, in a fuel-lean atmosphere. However, the space velocity was three times smaller than those used in this study. Zeolite based Pd–Ce catalysts showed 95% conversion after 40 h on stream, also for methane combustion [37]. Marceau et al. [38] observed sintering of Pt particles at 450 °C for the total oxidation of methane, but this was accompanied by an increase in the reaction rate. Initially, the sintering of the Pt particles improves the mobility of adsorbed oxygen, which can result in an increase of TOF, but eventually a decrease in the number of metal surface atoms results with a corresponding drop in the activity. It is believed that such a phenomenon happens here. As a comparison, it was also decided to test the long-term activity of our best Pt–Mo formulation, i.e. Mo_{comm} (Fig. 9). Even though this catalyst was previously exposed to just one reaction cycle, full conversion was not seen here until 660 °C. However, in a similar manner to its W equivalent, full conversion was obtained for the first 60 h of operation, after which a slight deactivation occurred, concluding with an activity of 97% after 100 h of operation. This was somewhat surprising because similar recent results from these laboratories [39] have shown

remarkable activity and stability for Mo promoted Pt/γ-Al_2O_3 catalysts for propane combustion. These catalysts were prepared (a) as described in Section 2 and (b) with highly regular, inverse opal microstructures.

The catalytic performance of Pt–Mo catalysts, relative to its Pt–W equivalents, in a fuel-lean environment, may also be affected by the formation of inactive Pt–Mo phases, evidence for this interaction was seen in the IR data. This phase can be easily oxidized to a catalytically active Pt–Mo-O_x species in the presence of oxygen [23], but it is clear that a larger excess of oxygen (λ here was 1.1) is necessary for this process to occur. However, in a fuel-rich environment, it is possible that these catalysts may show even more activity for methane combustion. The mechanisms of fuel-lean and fuel-rich catalytic combustion are very different [40]. The nature of the methane interaction with the surface of the catalyst changes as the state of the surface changes depending on fuel-rich or fuel-lean operation. It is possible that the catalyst can deactivate due to the ease of formation of PtO_2 in a fuel-lean environment. Operating under fuel-rich conditions renders the volatility of the catalyst inconsequential, allowing for a longer catalyst life. However, this is outside the scope of this publication. However, this issue is currently under investigation and will be addressed in the future.

4. Conclusion

Pt–W and Pt–Mo catalysts were evaluated for methane combustion using microreactor technology. W promoted catalysts show the most promise (of the two) for the catalytic combustion of methane. It is likely that the activity is a consequence of metal interaction effects between Pt° and W rather than the classical Pt°–Al_2O_3 interaction. For Pt–Mo catalysts, the extent of Pt dispersion appears to be the crucial factor. However, a detailed characterization study needs to be performed on both the sets of catalysts so as to elucidate the exact nature of these interactions. In conclusion, it can be said that bimetallic catalysts such as Pt/γ-Al_2O_3, promoted by W and Mo, show promise as effective catalysts for methane combustion under practical conditions.

References

[1] D.L. Trimm, Appl. Catal. 7 (1983) 249.
[2] R. Prasad, L.A. Kennedy, E. Ruckenstein, Catal. Rev. Sci. Eng. 26 (1984) 1.
[3] L.D. Pfefferle, W.C. Pfefferle, Catal. Rev. Sci. Eng. 29 (1987) 219.
[4] Z.R. Ismagilov, M.A. Kerzhenzev, Catal. Rev. Sci. Eng. 32 (1990) 51.
[5] M.F.M. Zwinkels, S.G. Järås, P.G. Menon, T.A. Griffin, Catal. Rev. Sci. Eng. 35 (1993) 319.
[6] T.V. Choudhary, S. Banerjee, V.R. Choudhary, Appl. Catal. A 234 (2002) 1.
[7] G. Kolb, V. Hessel, Chem. Eng. J. 98 (2004) 1.
[8] G.A. Petrachi, G. Negro, S. Specchia, G. Saracco, P.L. Maffettone, V. Specchia, Ind. Eng. Chem. Res. 44 (2005) 9422.
[9] P. Reuse, A. Renken, K. Haas-Santo, O. Görke, K. Schubert, Chem. Eng. J. 101 (2004) 133.
[10] G. Kolb, J. Schürer, D. Tiemann, M. Wichert, R. Zapf, V. Hessel, H. Löwe, J. Power Sources 171 (2007) 198.
[11] T. Seiyama, Catal. Rev. Sci. Eng. 34 (1992) 281.
[12] F. Zamar, A. Trovarelli, C. de Leitenburg, G. Dolcetti, J. Chem. Soc., Chem. Commun. 9 (1995) 965.
[13] H. Inoue, K. Sekizawa, K. Eguchi, H. Arai, Catal. Today 47 (1999) 181.
[14] P. Gelin, M. Primet, Appl. Catal. B 39 (2002) 1.
[15] Y. Yazawa, H. Yoshida, S. Komai, T. Hattori, Appl. Catal. A 233 (2002) 113.
[16] M. da Silva, M. Schmal, Catal. Today 85 (2003) 31.
[17] Z. Jiang, W. Huang, H. Zhao, Z. Zhang, D. Tan, X. Bao, J. Mol. Catal. A: Chem. 268 (2007) 213.
[18] V.K. Yatsimirskii, V.V. Lesnyak, I.N. Gut, O.Yu. Boldyreva, Theor. Exp. Chem. 41 (2005) 135.
[19] V.K. Yatsimirskii, V.V. Lesnyak, I.N. Gut, O.Yu. Boldyreva, Theor. Exp. Chem. 41 (2005) 271.
[20] W. Hua, J. Sommer, Appl. Catal. A 232 (2002) 129.
[21] R. Zapf, C. Becker-Willinger, K. Berresheim, H. Bolz, H. Gnaser, V. Hessel, G. Kolb, P. Löb, A.-K. Pannwitt, A. Ziogas, Trans. IChemE A 81 (2003) 721.
[22] G. Kolb, R. Zapf, V. Hessel, H. Löwe, Appl. Catal. A 277 (2004) 155.
[23] S. Hamada, S. Hibarino, K. Ikeue, M. Machida, Appl. Catal. B 74 (2007) 197.
[24] J. Weidlein, U. Müller, K. Dehnicke, Schwingungsfrequenzen II, Nebengruppenelemente, Georg Thieme Verlag, Stuttgart, 1986, p. 143.
[25] A. Duan, G. Wan, Z. Zhao, C. Xu, Y. Zheng, Y. Zhang, T. Dou, X. Bao, K. Chung, Catal. Today 19 (2007) 13.
[26] C. Hogarth, E. Assadzadeh, J. Mater. Sci. 18 (1983) 1255.
[27] O.S. Alexeev, S. Kawi, M. Shelef, B.C. Gates, J. Phys. Chem. 100 (1996) 253.
[28] J.S. M'Boungou, J.L. Schmitt, G. Marie, F. Garin, Catal. Lett. 10 (1991) 391.
[29] O.S. Alexeev, G.W. Graham, M. Shelef, B.C. Gates, J. Catal. 190 (2000) 157.
[30] H. Yoshida, Y. Yazawa, T. Hattori, Catal. Today 87 (2003) 19.
[31] R.F. Hicks, H. Qi, M.L. Young, R.G. Lee, J. Catal. 122 (1990) 280.
[32] M.H. Pinzón, A. Centeno, S.A. Giraldo, Appl. Catal. A 302 (2006) 118.
[33] G. Leclercq, S. Pietrzyk, T. Romero, A. El Gharbi, L. Gengembre, J. Grimblot, F. Aissi, M. Guelton, A. Latef, L. Leclercq, Ind. Eng. Chem. Res. 36 (1997) 4015.
[34] P. Gelin, L. Urfels, M. Primet, E. Tena, Catal. Today 83 (2003) 45.
[35] R. Burch, P.K. Loader, Appl. Catal. B 5 (1994) 149.
[36] A.L. Barbosa, J. Herguido, J. Santamaria, Catal. Today 64 (2001) 43.
[37] C. Shi, L. Yang, J. Cai, Fuel 86 (2007) 106.
[38] E. Marceau, M. Che, J. Saint-Just, J.M. Tatibouët, Catal. Today 29 (1996) 415.
[39] G. Guan, R. Zapf, G. Kolb, Y. Men, V. Hessel, H. Loewe, J. Ye, R. Zentel, Chem. Commun. 3 (2007) 260.
[40] M. Lyubovsky, L.L. Smith, M. Castaldi, H. Karim, B. Nentwick, S. Etemad, R. LaPierre, W.C. Pfefferle, Catal. Today 83 (2003) 71.